Correlation between the dynamics of nanoconfined water and the local chemical environment in calcium silicate hydrate nanominerals

Valentina Musumeci, Guido Goracci, Paula Sanz Camacho, Jorge Dolado, Cyril Aymonier

FULL PAPER

Correlation Between the Dynamics of Nanoconfined Water and Local Chemical Environments in Calcium Silicate Hydrate Nanominerals

Valentina Musumeci,[a, b] Guido Goracci,[b, c] Paula Sanz Camacho,[a] Jorge S. Dolado,*[b, d] Cyril Aymonier*[a]

[a] V. Musumeci, Dr. P. Sanz Camacho, Dr. C. Aymonier
CNRS, Univ. Bordeaux, Bordeaux INP, ICMCB, UMR 5026
F-33600 Pessac (France)
E-mail: cyril.aymonier@icmcb.cnrs.fr
[b] V. Musumeci, Dr. G. Goracci, Dr. J.S. Dolado
Centro de Física de Materiales (CSIC-UPV/EHU)-Materials Physics Center (MPC)
Paseo Manuel de Lardizabal 5, 20018 San Sebastián (Spain)
E-mail: jorge_dolado002@ehu.eus
[c] Dr. G. Goracci
BASKRETE-Euskampus Fundazioa,
Ed. Rectorado Barrio Sarriena s/n, 48940 Leioa (Spain)
[d] Dr. J.S. Dolado
Donostia International Physics Center (DIPC),
Paseo Manuel Lardizábal 4, 20018 Donostia-San Sebastián (Spain)

Supporting information for this article is given via a link at the end of the document.

Abstract: Calcium silicate hydrates are members of a large family of minerals with layered structures containing hanging Ca-OH and Si-OH groups that interact with confined water molecules. To rationalize the impact of the local chemical environment on the dynamics of water, Si-OH-rich and Ca-OH-rich model nanocrystals were synthesized using the continuous supercritical hydrothermal method and then systematically studied by a combination of spectroscopic techniques. In our comprehensive analysis, the ultrafast relaxation dynamics of hanging hydroxyl groups can be univocally assigned to Ca-OH or Si-OH environments, and the local chemical environment largely affects the H-bond network of the solvation water. Interestingly, the ordered “ice-like” solvation water found in the Si-OH-rich environments is converted to a disordered “liquid-like” distribution in the Ca-OH-rich environment. This refined picture of the dynamics of confined water and hydroxyl groups in calcium silicate hydrates can also be applied to other water-containing materials, with a significant impact in many fields of materials science.

Introduction

Understanding the dynamics of nanoconfined water, especially in terms of molecules trapped in nanocavities or strongly bonded to the material surface, is a theme of great interest across numerous scientific fields[1–8]. The features of nanoconfined water are highly dependent on the surface interactions and confinement geometry and are further modified by the presence of different chemical environments.[9,10] In this context, $CaO\text{-}SiO_2\text{-}H_2O$ minerals represent an extremely good system for investigating the effect of the chemical network surrounded by the water molecules. This family of minerals consists of approximately thirty different layered crystalline structures with different calcium-to-silicon (Ca/Si) ratios containing intrinsic interlayer water. Calcium silicate hydrate minerals can form in nature as a consequence of geological hydrothermal processes in which hyperalkaline fluids react with basic igneous rocks or as a product of chemical reactions that take place during cement hydration. In the latter case, the calcium silicate hydrate (C-S-H) gel represents the principal hydration product of cement paste. The extensive interest in the study of this system is due to the strong influence of the water molecules at the microscopic scale on the macroscopic properties of the cement, such as resistance, strength and durability.[11] At the microscale, C-S-H gel adopts a semi-amorphous phase consisting of $Ca(OH)_2$ layers and isolated silicate chains with variable lengths and numbers of hydroxyl units attached to Si atoms linked by water molecules. This material is characterized by short-range order, variable stoichiometry and a Ca/Si ratio ranging from 0.7 to 2.3.[12] A general formula for describing C-S-H gels is $Ca_xH_{2(N+1-x)}Si_NO_{(3N+1)}\cdot zCa(OH)_2\cdot mH_2O$, where N is the silicate chain length, 2(N+1-x) is the number of –OH groups linked to the chain and *z* is the number of calcium hydroxide units surrounded by *m* water molecules.[13] Several previous studies have investigated the dynamics of nanotrapped water in C-S-H materials using different experimental techniques. Among these techniques, broadband dielectric spectroscopy (BDS) is a nondestructive experimental technique commonly used for the investigation of the dynamics of confined water, [14,15] in both biological systems, [16-18] and porous materials (such as clays, [19-22] molecular sieves, [23-26] and zeolites[27,28]). In fact, due to its large frequency (10^{-6}-10^{12} Hz) and temperature (100-670 K) ranges, this technique allows us to explore the dynamic features of water over an extremely broad time range, from 10^2 to 10^{-8} s. [29] In the literature, three main water dynamics were observed in C-S-H gel in the supercooling region (100 K-250 K). [11,30] The weak and broad components at low temperature (110 K) were independent of the amount of water and were the only dynamics observed in the sample dried at 120 °C; for these reasons, this contribution was associated with the dynamics of hydroxyl groups. On the other hand, the processes observed at a higher temperature (190 K) presented dynamical features typical of water in confined systems and,
consequently, were associated with the dynamics of water molecules in the small and large pores of C-S-H.

Apart from the study of nanotrapped water in this material, the only other study on calcium silicate hydrate minerals is an investigation of tobermorite. Tobermorite is an analogous crystalline form of C-S-H gel and is thus an excellent model system for mimicking the C-S-H properties. The ideal structure of tobermorite ($Ca_{4+x}Si_6O_{15+2x}(OH)_{2-2x}\cdot 5H_2O$, with x ranging from 0 to 0.5 and a Ca/Si molar ratio equal to 0.83) consists of a double silicate chain between layers of 7-coordinate calcium cations, and thus, the tobermorite structure contains only Si-OH units. [31,32] *Monasterio et al.* compared the BDS results of natural and synthetic tobermorite (synthesized at 200 °C in 4 h). [33] Unlike in previous works on C-S-H, a well-defined contribution to the dielectric response was observed at low temperature (110 K) in both the natural and synthetic materials. As evidenced by the different shapes of this contribution in the dielectric spectra of C-S-H and tobermorite, and the presence of aluminum in the tobermorite samples, aluminum helped to stabilize synthetic tobermorite, it was suggested that the origin of this component was related to the dynamics of water confined in aluminum-rich zeolite cavities. On the other hand, at a higher temperature, the process behavior was similar to that observed for water molecules in small C-S-H gel pores.

Despite all these previous studies, the definitive origin of the relaxation processes in these systems is difficult to ascertain, and an appropriate assignment is still incomplete. This lack of knowledge can be attributed to two main reasons. First, the description of the C-S-H gel, which accommodates both Ca-OH and Si-OH groups at the nanoscale, is very complex due to its heterogeneous and amorphous nature. Second, the tobermorite mineral, even if more crystalline, contains only Si-OH groups and thus does not allow us to investigate the effect of different chemical environments on the dynamics of water molecules.

In this scenario, it is clear that a complete understanding of the nanoconfined water dynamics is possible only by comparison of two highly crystalline materials characterized by different surface topologies that depend on the presence of Ca-OH and Si-OH groups. Tobermorite is an optimal candidate to explore the effect of the Si-OH environment on water dynamics, and xonotlite is expected to be a good mineral archetype to study the further contribution of the Ca-OH chemical environment. Xonotlite (Ca/Si molar ratio equal to 1) is a calcium silicate hydrate mineral naturally and hydrothermally connected to tobermorite. Xonotlite has an ordered layer structure in which Si_6O_{17} double chains bond via sheets of edge-sharing Ca-polyhedra, and unlike those of tobermorite, the OH groups are located at the free apices of the calcium octahedra. Xonotlite is usually described as having the following ideal stoichiometric formula $Ca_6Si_6O_{17}(OH)_2$.[34,35] However, several studies have shown that both natural and synthetic xonotlite contain excess water, which is present partially as Si-OH groups and partially as molecules.[34,36,37] As a consequence, the exact chemical formula should be closer to $(CaOH)_2Ca_{3.6}(H_{0.8}Si_6O_{17}) \cdot m\ H_2O$, with $m \leq 2$, as suggested by *Grimmer et al.* [38]

This work aims to further elucidate the relation between the dynamics of nanoconfined water and the local material chemistry in calcium silicate hydrates by considering two appropriate synthetic model nanominerals in which the processes can be rigorously ascribed. In order to do that, highly crystalline tobermorite and xonotlite as models have been synthesized by employing an innovative supercritical water-based technology, which allows fine control of the chemical structure of the materials by tuning the Si-OH and Ca-OH contents. [39] Moreover, for the first time, an in-depth characterization of these model nanominerals using a combination of sophisticated spectroscopic techniques allowed us to univocally refine the picture of the water dynamics in these systems. As it will be shown later in this work, the local chemical environment of nanominerals (either Ca-OH or Si-OH) has a profound effect on both the dynamic and structural characteristics of water molecules and hydroxyl groups.

Results and Discussion

Structural characterization of model xonotlite and tobermorite

PXRD was used to identify the mineral phases and to investigate the crystallinity of the materials. In Figure 1a, the X-ray diffraction pattern shows well-defined peaks coincident with those of tobermorite (pdf 01-083-1520), confirming the high crystallinity of the tobermorite phase. It must be emphasized that we are synthesizing tobermorite at a temperature (400 °C) far above its stability limit, which is approximately 140 °C. [47] The formation of a thermodynamically unstable phase under the synthesis conditions, namely, tobermorite, is allowed because of the fine control of the reaction kinetics under supercritical conditions (400 °C and 25.0 MPa). However, the X-ray diffraction pattern in Figure 1b indicates that the material is xonotlite (pdf 00-023-0125) when the synthesis occurs with another Ca/Si ratio of 1 in supercritical water under the same temperature and pressure of 400 °C and 25.0 MPa.

The morphology of the obtained minerals was investigated by SEM. As shown in Figure 1c, tobermorite continuously synthesized in supercritical water exhibits a fiber-like morphology with a size of approximately 1-20 μm in length and 10-20 nm in width. This result confirms the similarity of the “supercritical” tobermorite to the natural mineral, which also crystallizes in the form of fibers or plates[48]. In contrast, tobermorite prepared by conventional hydrothermal synthesis shows a foil-like morphology unless templates are employed to induce fiber formation.[48,49]

Xonotlite crystals, as shown in Figure 1d, mainly consist of tiny flat fibers that are approximately 1-30 μm long and 50-100 nm wide. Previously, Lin and coworkers reported similar results for synthetic xonotlite prepared by conventional hydrothermal treatment at 200 °C for 24 hours. [50]

Regarding the FTIR measurements, the characteristic absorption spectra of xonotlite and tobermorite are shown in Figure 2. In the range of OH stretching frequencies from 1500 to 4000 cm^{-1}, both spectra show a broad band at approximately 3400 cm^{-1}, which is presumably linked to the stretching contributions of both structurally incorporated OH groups and surface-adsorbed water ($Si\text{-}OH\cdots H_2O$), as reported in the simulation results of Churakov and coworkers. [51] A more intense peak attributed to adsorbed and interlayer water is observed in the tobermorite phase rather than in xonotlite. Furthermore, it is interesting to highlight the similarity of our results for “supercritical” tobermorite with those reported by Monasterio and coworkers for natural tobermorite. [33] In this work, the FTIR

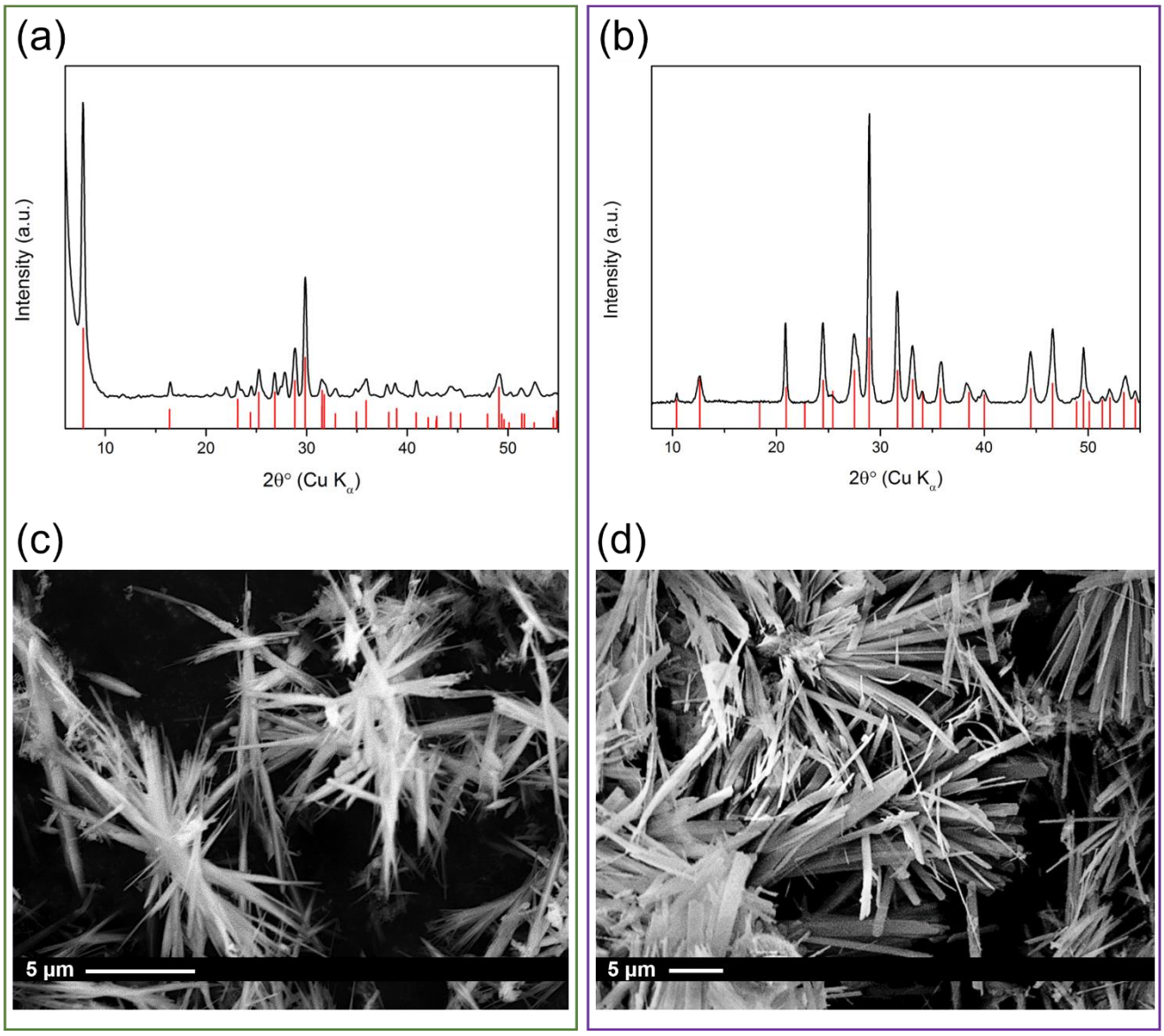

Figure 1. X-ray diffraction patterns and SEM images of tobermorite, (a) and (c), respectively, and xonotlite, (b) and (d), respectively, synthesized in supercritical water at 400 °C and 25.0 MPa. The red lines in (a) and (b) represent the reference pdf 01-083-1520 and pdf 00-023-0125 used to identify tobermorite and xonotlite, respectively.

spectra of natural and “subcritical” samples (synthesized at 200 °C in 4 hours) were compared, highlighting a shift toward lower wavenumbers of the broad peak attributed to OH in the natural specimen. Such an effect was related to the higher crystallinity in the natural network, which reduced the strength of the OH bond. [33] The sharp absorption peak at 3610 cm^{-1} is attributed to the Ca-OH vibration and appears only in the spectrum of xonotlite; this bonding is exclusively contained in the xonotlite structure and thus is characteristic of this mineral.

In the range of 400-1500 cm^{-1}, the presence of numerous overlapping bands is attributed to the coupled stretching and bending of octahedral Ca and tetrahedral Si.[51] These bands are characteristic and common to many calcium silicate hydrates. The Si-O stretching modes of tobermorite are more overlapped and less defined than those of xonotlite.

The position of the peaks in the spectra of both xonotlite and tobermorite and the origin of each resonance are summarized in Table 1.

A full comprehension of the hydrogen bond network in xonotlite and tobermorite has been obtained with further investigation in the 2800-3800 cm^{-1} region by micro-Raman spectroscopy. The spectrum of xonotlite (Figure 3) shows two groups of Raman-active vibrations. The most intense and sharp signal, centered at 3611 cm^{-1}, is attributed to Ca-OH stretching bands of hydroxyl units in the mineral, similar to those of portlandite ($Ca(OH)_2$), where this mode appears at 3618 cm^{-1}. [55]

At lower frequencies, the broad band centered at approximately 3500 cm^{-1} is assigned to OH stretching vibrations of surface-adsorbed water molecules, in agreement with the FTIR results. In contrast, the Raman spectrum of tobermorite (Figure 3) shows only one broad signal centered at approximately 3480 cm^{-1}. This band is attributed to water stretching vibrations and has a much greater intensity than that in xonotlite.

The Raman results confirm, as already suggested from FTIR, the absence of hydroxyls linked to the Ca-O sheets in the tobermorite

structure. These results are in agreement with the results of several studies on natural minerals and confirm that both xonotlite and tobermorite prepared in SCW exhibit structural characteristics similar to those of natural minerals. [55-57]

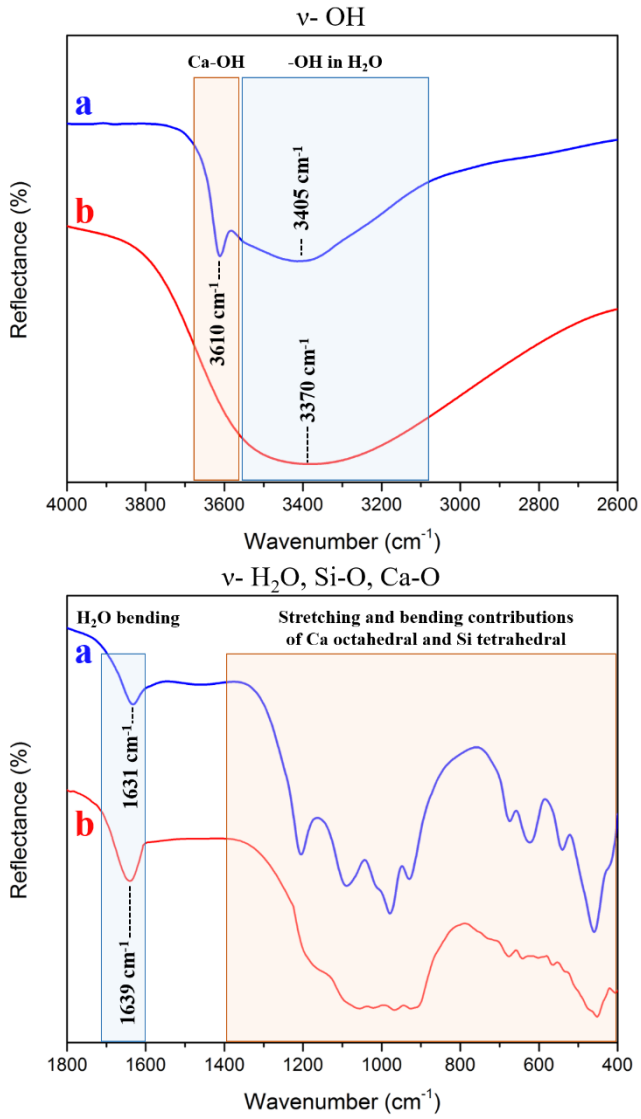

Figure 2. FTIR spectra of (a) xonotlite and (b) tobermorite synthesized in supercritical water.

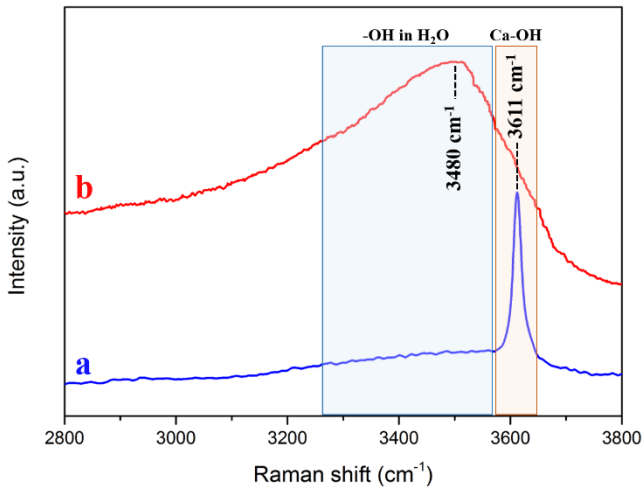

Figure 3. Raman spectra of (a) xonotlite and (b) tobermorite synthesized in supercritical water.

^{1}H MAS NMR was used to explore the local environment of protons at the atomic nearest neighbor and next-nearest neighbor scale. The xonotlite spectrum was deconvoluted into four signals (fitted curves) centered at 1.9 ppm, 2.3 ppm, 5.1 ppm and 15.2 ppm, as shown in Figure 4a. The sharp peaks at 1.9 and 2.3 ppm are attributed to the presence of Si-OH and Ca-OH bonds, respectively, while the broad signal at 5.1 ppm can be assigned to molecular water adsorbed on the xonotlite particle surface. These results are in agreement with the existence of different types of proton environments already detected in both natural and synthetic xonotlite synthesized under conventional and hydrothermal conditions. [34,37,51,58]

Last, the peak at 15.2 ppm can be assigned to strongly hydrogen-bonded protons involving Si-OH groups, as already observed in other silicate minerals. [59]

To our knowledge, in literature there is any study that focuses on the local environment of hydrogen species in tobermorite structure determined through ^{1}H MAS NMR. Peak assignments and data analysis are a challenge due to the complexity of the structure and the multiplicity of possible proton configurations. In Figure 4b, the ^{1}H MAS NMR spectrum of tobermorite formed in SCW exhibits two sharp peaks centered at 1.2 ppm and 3.7 ppm and three broad shoulder signals at 2.2 ppm, 5 ppm and 12.8 ppm. All these peaks are related to the presence of structural OH and molecular water as well as interlayer water in tobermorite. Despite the similarity of the xonotlite and tobermorite structures, the comparison between the ^{1}H MAS NMR spectra shows several differences.

First, the slight shift toward higher values of Si-OH groups in xonotlite (1.9 ppm) rather than in tobermorite (1.2 ppm).

This experimental evidence could be explained by considering that hydroxyl groups with stronger hydrogen bonding exhibit larger chemical shifts than those with weaker hydrogen bonding.[60] Thus, the downfield shift of the Si-OH bond peak in the tobermorite spectrum occurs mainly due to the decrease in the electronic charge on the hydrogen bonded proton. This result is in accordance with previous studies on silica particles, which reported the observation of a peak at 1.1 ppm assigned to isolated (i.e., not hydrogen bonded) silanols at the SiO_2 surface. [61] Therefore, the intense peak at 1.2 ppm can be assigned to protons in structural and weakly bonded Si-OH groups. On the other hand, the peak at 2.2 ppm can be assigned to protons linked to Ca-O, in accordance with the results reported by Colombet and coworkers (2.4 ppm) for numerous polycrystalline calcium hydrosilicate materials.[62] Furthermore, the findings of Colombet's study show that the typical range for protons in water molecules is from 3 ppm to 6 ppm.[62] Water molecules within minerals can be present in zeolitic sites or interlayer regions, as well as on the surface in the form of macroscopic fluid inclusions or microscopic cracks in the crystal.[63]

Yesinowski and coworkers investigated numerous hydrous species in minerals by ^{1}H MAS NMR and reported that only minerals, such as analcite and hemimorphite, containing hydrogen in the form of stoichiometric amounts of water showed peaks at approximately 3.1 and 3.6 ppm.[63] These chemical shift values are very close to the value of 3.7 ppm found in this work. Consequently, this peak appearing in the tobermorite spectrum and absent from that of xonotlite is probably related to the presence of stoichiometric amounts of water located in the cavities between double silicate chains.

Table 1. FTIR peak assignments for xonotlite and tobermorite synthesized in supercritical water**.**

Peak Position (cm^{-1})		Assigned vibration
Xonotlite	Tobermorite	
3610	-	Ca-OH [45]
3405	3370	stretching contributions of structurally incorporated OH groups and surface adsorbed water [45,46,53]
1631	1639	H_2O bending [46,51,54]
1204	Broad shoulder ~1200	Si-O stretching (O-links between bridging tetrahedral)[46,51,52,54]
1088	Broad shoulder ~1060	Si-O-Si symmetric stretching modes [46,51,52,54]
978	970	Si-O symmetric stretching modes [45,46]
673	677	Si-O-Si bending [46,51,52,54]
625	-	Ca-OH bending mode [45]
456	452	O-Si-O out-of-plane rocking motion-deformation of tetahedra [46,52]

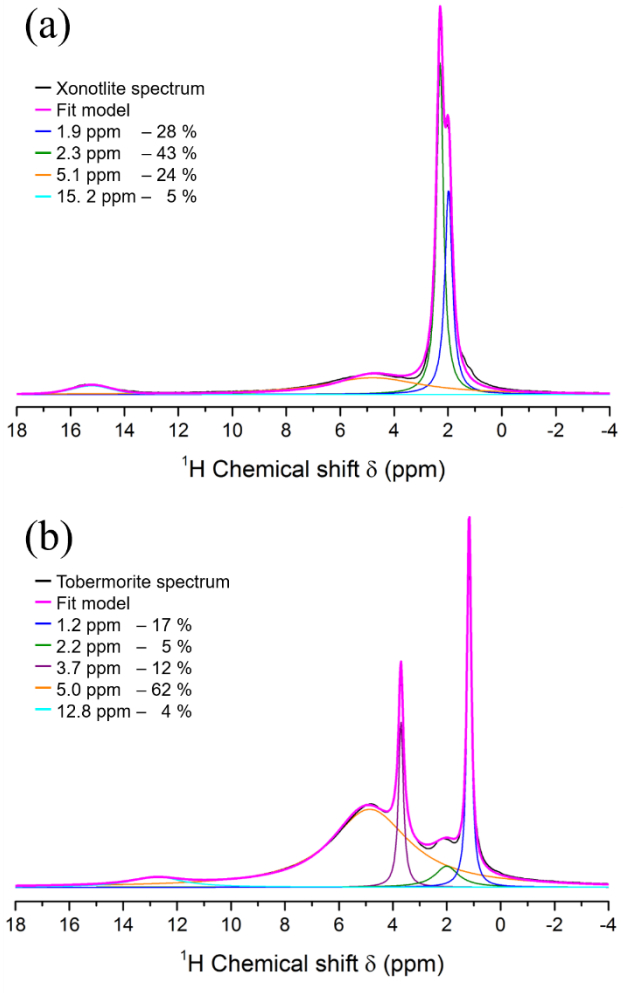

Figure 4. ^{1}H MAS NMR spectra of (a) xonotlite and (b) tobermorite. The fitted curves together with the respective contribution percentage are reported.

Finally, as for xonotilte, the resonances at 5.0 ppm and 12.8 ppm arise from water on strongly hydrated surfaces and strongly hydrogen-bonded protons in Si-OH groups, respectively. [58,59,61,64]

Dielectric response of model xonotlite and tobermorite formed in SCW

In a typical dielectric experiment, the response of the material to an external electric field is measured.[29] The polarization inside the sample can be induced by different mechanism such as (i) charge displacement, (ii) orientational polarization, and (iii) redistribution of free charges. Therefore, measurements of complex permittivity ($\varepsilon^*(\omega) = \varepsilon'(\omega) - i\varepsilon''(\omega)$) allow us to investigate the dynamics of dipolar species as well as charge transport. In the case of minerals with analogous distributions of hydrous species in the structure, such as xonotlite and tobermorite, water molecules and hydroxyl groups are expected to contribute to the dielectric signal in a similar way. However, the BDS analysis, conducted on xonotlite for the first time in this work, revealed some specific and different properties between the two mineral structures that cannot be detected with other conventional techniques. In Figure 5, the imaginary part of the tobermorite and xonotlite complex permittivity (ε'') is shown at representative temperatures (100 K, 160 K and 200 K). Starting from the low-temperature region, the tobermorite signal is characterized by a well-defined peak (P1), as shown in Figure 5a. In Figure 5b, xonotlite shows two components at the same temperature, slower (P1S) and faster (P1F) than that observed in tobermorite. Upon increasing the temperature, a new weak process is observed in both samples (P2). Finally, at higher temperatures, process P3 enters the frequency range of the dielectric spectrometer, as shown in Figure 5c and 5d. All the processes shift toward higher frequencies as the temperature increases, suggesting that the process is thermally activated.

To extract information about the relaxation times, the dielectric response can be described by using standard fit functions. In that case, as commonly done for confined water, the data were analyzed in terms of Cole-Cole functions[65] that are defined as (Equation 1):

$$\varepsilon^*(\omega) = \varepsilon_\infty + \frac{\Delta\varepsilon}{1+(i\omega\tau)^\alpha} \quad (1)$$

where $\Delta\varepsilon = \varepsilon_S - \varepsilon_\infty$ is the relaxation strength (with ε_S and ε_∞ the relaxed and unrelaxed values of the dielectric constant, respectively), τ is the characteristic relaxation time, ω is the angular

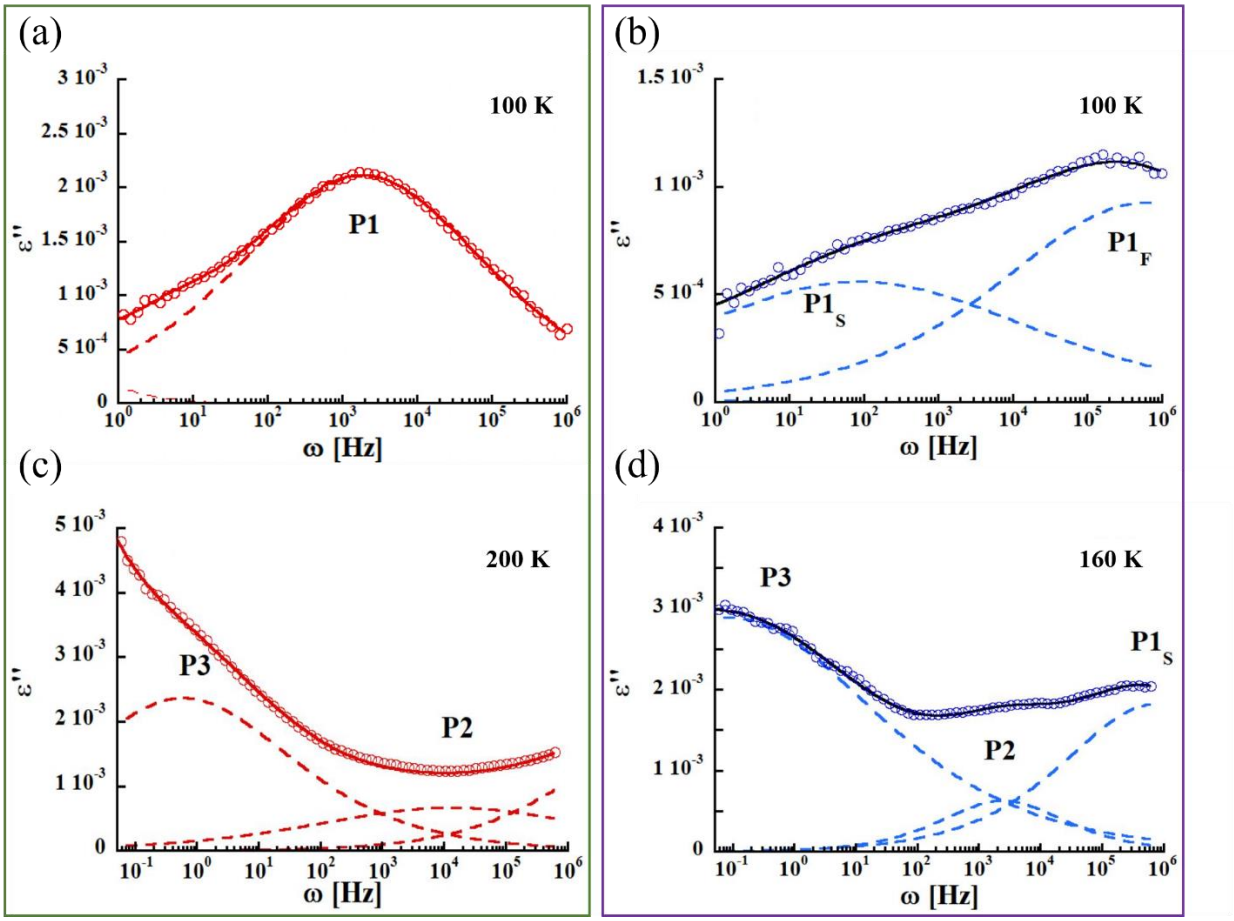

Figure 5. Imaginary part (ε″) of the dielectric spectra of nanominerals at different temperatures: tobermorite at (a) 100 K and (c) 200 K and xonotlite at (b) 100 K and (d) 160 K. The solid lines represent the fits to the experimental data. The dashed lines represent the relaxation corresponding to processes 1, 2, and 3.

frequency, and *α* is the shape parameter that determines the symmetric broadening of the relaxation peak ($0 < \alpha \leq 1$).

In Figure 6, the temperature dependence of the extracted relaxation times for each dynamic observed in tobermorite and xonotlite is shown.

All the processes show an Arrhenius-type temperature dependence within the entire temperature range, in accordance with:

$$\tau = \tau_0 \, e^{\frac{E_a}{K_B T}} \quad (2)$$

where the pre-exponential factor τ0 and the activation energy (E_a) provide information about the nature of the motions involved in relaxation processes (see Table 2). Starting from the faster process, P1 is characterized by a low energy activation (between 0.12 and 0.18 eV) and a characteristic time $\tau_0 \sim 10^{-12}$ s typical of vibrational dynamics. A similar process was previously observed in the investigation of natural and synthetic tobermorite by *Monasterio et al.* [33,66] In that work, this process was associated with the fast dynamics of water molecules in aluminum-rich zeolitic cavities. However, xonotlite does not have this kind of cavity; therefore, such interpretation is not consistent with the results obtained in our work. Moreover, in this time and temperature range, a broad and weak contribution was found even in silica nanoparticles[67] and other cementitious materials, synthetic C-S-H and a cement matrix. [11,30]

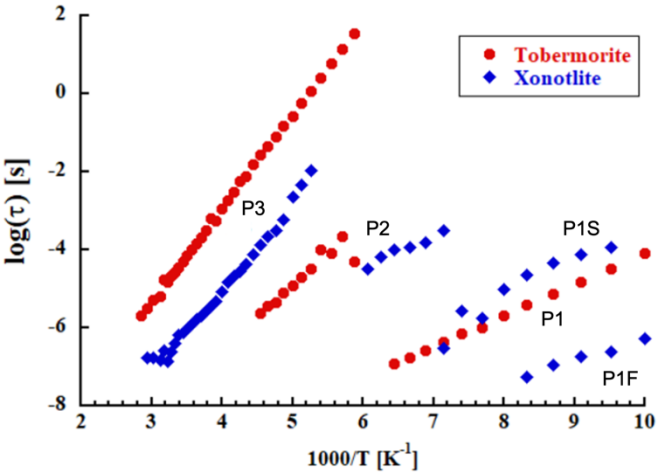

Figure 6. Temperature dependence of relaxation times related to the observed dynamics in tobermorite (filled red circles) and xonotlite (filled blue diamonds) formed in the SCW.

Table 2. Activation Energy, E_a, and pre-exponential factor, log (τ_0), obtained from the Arrhenius equation applied to the data in Figure 6.

Material	Process 1		Process 2		Process 3	
	E_a (eV)	log τ_0(s)	E_a (eV)	log τ_0(s)	E_a (eV)	log τ_0(s)
Xonotlite	0.12 P1F	-12.0 P1F	0.16	-9.3	0.42	-13.5
	0.18 P1S	-12.2 P1S				
Tobermorite	0.16	-12.1	0.33	-13.3	0.48	-12.6

In particular, in the latter systems, the origin of this contribution was associated with the rotational dynamics of hydroxyl groups. Considering that it is generally accepted that the C-S-H phase has a tobermorite-like structure, [68-71] we suggest that process 1 is related to the dynamics of hydroxyl groups. The well-defined shape of this component can be attributed to the ordered distribution of OH groups on tobermorite layers, while, as we add defects to the structure, the disordered environment is reflected in the broadening of process P1. To understand the differences observed in tobermorite and xonotlite, we must recall the ^{1}H NMR results. In the xonotlite spectrum, we observed a double peak related to the presence of two different populations of hydroxyl groups, Ca-OH and Si-OH, while in the tobermorite spectrum, a single peak was observed at a lower chemical shift associated with isolated silanol groups. Hence, the presence of two P1 processes in xonotlite can be related to the presence of two hydroxyl group populations with different chemical environments. Regarding process 2, the results obtained by the Arrhenius fitting procedure suggest a different nature and origin of this process in tobermorite and xonotlite (see Table 2). In fact, in tobermorite, these dynamics show energy activation and characteristic times similar to those of the strongly bound water already observed in several dried or low-relative-humidity systems, such as titanate nanowires,[72] zeolites,[25,28] hydrocalumites[73] and silica nanoparticles (SNPs)[67]. According to the ^{1}H NMR results, only tobermorite exhibits the characteristic peak related to hydrated hydroxyl groups. Therefore, we might expect a scenario similar to that studied by Cerveny *et al.* in SNPs dried at 373 K, and P2 can be associated with the dynamics of water molecules hydrating the silanol groups.[67]

On the other hand, in xonotlite P2 has a lower activation energy, and $\tau_0 \sim 10^{-9}$ s suggests a diffusional nature of this process, while $\tau_0 \sim 10^{-13}$ s is characteristic of a vibration dynamic. This different behavior can be related to a distinct interaction between water molecules and the surface of the layer, as already observed by ^{1}H NMR. *Sulpizi et al*. have shown that the orientation and distribution of hydroxyl groups on the surface of SiO_2 affect the arrangement of water molecules on the surface.[74] In particular, according to those authors, it is possible to have a "liquid-like" distribution of water molecules instead of the more ordered "ice-like" distribution. Since process 2 is normally associated with the presence of a tetrahedrally coordinated distribution of water molecules, the diffusive behavior dynamics in xonotlite indicate the absence of such water coordination. We suggest that the presence of Ca-OH affects the distribution of hydroxyl groups on the surface of xonotlite, giving rise to a more disordered arrangement of water molecules, that is, "liquid-like", where a diffusive dynamic appears to be more favorable than the typical vibration behavior observed in tobermorite. Finally, process P3 has a similar activation energy and pre-exponential factors, suggesting that it originates from the same dynamics in both tobermorite and xonotlite. However, in xonotlite, the relaxation times are three orders of magnitude faster than those in tobermorite. A process with values of τ_0 and relaxation times similar to those found in this work has been observed even in zeolites.[25,28] In these studies, such dynamics were related to the migration of cations in supercages.

Finally, contributions from charge migration in the same frequency and temperature range have been observed in titanate nanowires[72] and CaFe-layered double hydroxide[73]. In this scenario, the faster dynamics observed in xonotlite can be explained by the higher content of nonevaporable water detected trough TGA measurement in the range between 105 and 300 °C, as shown in Figure S1. In fact, the double amount of nonevaporable water in xonotlite, c_w = 0.95 wt%, respect to tobermorite, c_w = 0.48 wt%, enhances the cation mobility, resulting in a shift toward smaller relaxation times.[75]

Conclusion

The dynamics of confined water in nanominerals are highly dependent on the interactions and confinement geometry and are modified by the presence of different chemical environments. In this work, the water dynamics in two calcium silicate hydrate minerals, xonotlite and tobermorite, have been thoroughly studied. Despite the similarities in their stoichiometric and morphological layered structures, the chemical environments of xonotlite and tobermorite minerals are dominated by Ca-OH and Si-OH groups, respectively. On the basis of a combination of spectroscopic techniques such as Raman, FTIR, solid-state NMR and BDS, a refined picture of the dynamics of water in calcium silicate hydrates was possible, allowing univocal assignments of each dielectric relaxation process to a specific structural origin. The fastest relaxation dynamic (P1) found in the calcium silicate hydrate phases was previously hypothesized to arise from the hanging hydroxyl ions, but this work confirms this assignment by distinguishing the Ca-OH and Si-OH environments. In addition, our results reveal that the second fastest processes (P2) are intimately related to hydration/solvation water dynamics and that these processes are very sensitive to the local chemical environment. In that respect, the ordered "ice-like" solvation water found in the Si-OH-rich environments of tobermorite transforms into a disordered "liquid-like" solvation water found in the Ca-OH-

enriched environment of xonotlite. Finally, our experiments suggest that the slowest process (P3) is related to bulky nonevaporable water and coupled to ion mobilities. Overall, this work might serve as a starting point for understanding the water dynamics in more complex calcium silicate hydrates, such as cementitious C-S-H gel, and provide a solid fundamental knowledge body for other water-containing materials. Another extension of this work is to disclose the effect of the water content on the dynamics of the different contributions.

Experimental Section

Synthesis method

Above its critical point (374 °C and 22.1 MPa), supercritical water (SCW) exhibits unique physiochemical properties, such as density, viscosity, and dielectric constant, which differ largely from those of water under ambient conditions.[40,41] The use of SCW results in high reaction rates and increased nucleation of inorganic materials, allowing replacement of costly, hazardous, and polluting organic solvents.[42,43] This sustainable and scalable methodology, due to its versatility, offers the possibility to finely adjust the process parameters and the reaction kinetics. Consequently, supercritical hydrothermal flow synthesis is particularly useful to manipulate, as desired, the reaction environment for application in materials processing.[39,44] In the context of C-S-H production, the main advantage of this technique is the ultrafast reaction kinetics: it is possible to synthesize crystalline calcium silicate hydrate nanoparticles, such as xonotlite and tobermorite, in a few seconds in continuous mode.[45,46] Furthermore, it should be emphasized that the supercritical C-S-H minerals are more similar, in terms of morphology, crystallinity and structure, to the natural phases than to the synthetic minerals reported so far in the literature. This experimental evidence suggests that in addition to the reduced synthesis times, this innovative technology more accurately captures the formation process that takes place in nature.

Characterization techniques

X-ray diffraction

The powder X-ray diffraction (PXRD) patterns were collected by using a PANalytical X'Pert PRO powder X-ray diffractometer with the Bragg-Brentano θ-θ geometry. The radiation source, Cu-K_α radiation (λ = 1.5418 Å) was operated at a generator voltage of 45 kV and a current of 40 mA. Continuous scans were recorded over the angular range from 5.01 to 69.98° (2θ) with a minimum step size of 0.016° (2θ). Prior to measurement, the samples were finely ground into a powder and passed through a 100 µm mesh sieve.

Scanning electron microscopy

The particle size and morphology of the materials were investigated by scanning electron microscopy (SEM) with a Jeol JSM 6360A microscope. The electron beam was operated in the voltage range of 0.4-40 kV, allowing a magnification between 10× and 300 000×. For the analysis, the dry powder samples were placed in an aluminum stub by using two-sided carbon tape. Prior to imaging, as C-S-H minerals are nonconductive materials, an electrically grounded layer of gold was deposited on the surface by sputter coating. The metal coating improved the conductivity of the sample, thus minimizing the negative charge accumulation of the electron beam.

Fourier transform infrared spectroscopy

Fourier transform infrared (FTIR) spectroscopy was performed using a Bruker Equinox 55 FTIR spectrometer. The measurements were conducted in the 400 - 4000 cm^{-1} spectral absorption region at room temperature. Thirty-two scans were collected for each sample with a spectral resolution of 4 cm^{-1}. For the analysis, the sample (1 wt.%) was dispersed into an appropriate amount of KBr, which is optically transparent within the mid-IR region. The sample and KBr were ground to reduce the particle size to less than 5 mm in diameter and to avoid scattering of the infrared beam.

Raman spectroscopy

The vibrational properties of xonotlite and tobermorite crystals were characterized using a Raman spectrometer (HORIBA Jobin-Yvon Xplora). The system was equipped with a laser of excitation wavelength and spot size equal to 532 nm and ~ 1 µm, respectively. Prior to analysis, the instrument was calibrated using the 520.5 cm^{-1} line of a silicon wafer. The measurements were performed using a 100× objective, a grating with 2400 lines/mm and a CCD detector. Repeated acquisition of the spectra in the 2800 - 3800 cm^{-1} range with an exposure time of 30 s was performed to improve the signal-to-noise ratio.

Solid-state nuclear magnetic resonance spectroscopy

Solid-state nuclear magnetic resonance (SSNMR) spectra were acquired on a Bruker Avance 300 MHz spectrometer, equipped with a 7.05 T wide bore magnet. The experiments were performed at room temperature using a standard 4-mm magic angle spinning (MAS) probe with MAS rates of 10 kHz. A rotor-synchronized Hahn-echo sequence was employed with a π/2 pulse of 2 µs and a recycle delay of 5 or 10 s. Chemical shifts are referenced relative to ultrapure Milli-Q water (shift: + 4.7 ppm).

Thermal analysis

Thermogravimetric analysis (TGA) was performed using a TA Instruments Q500 at a heating rate of 5 K/min under nitrogen flow. Before the measurement, 15 minutes of isothermal nitrogen flow at room temperature was carried out for each sample.

Broadband dielectric spectroscopy

The measurement of the complex dielectric permittivity was determined by a Novocontrol Alpha-N broadband dielectric spectrometer in the frequency range of 10^{-2} - 10^{6} Hz. The isothermal frequency scans were recorded every 5 degrees within a temperature range of 100-300 K. At higher temperatures, the isothermal frequency scans were performed in 10 K increments. During the experiment, the sample temperature was kept stable within 0.1 K by nitrogen gas flow. To date, BDS has been applied to cement-based materials, with a focus on the dynamic features of bulk water. However, as the signal from these water molecules is very intense, the dynamics of the structural water are generally hidden; therefore, information on this population is lost. As we are mainly interested in the structural differences between xonotlite and tobermorite, prior to measurement, the samples were dried at 105 °C for 1 h inside the dielectric cell cryostat of the experimental equipment to remove the evaporable water content and focus attention on the dynamics of nanoconfined water.

Acknowledgements

This research was carried out under the umbrella of the Bordeaux-Euskampus Euro-regional Campus of International Excellence initiative and supported by the International Doctoral Program developed between the University of Bordeaux (UB) and the University of the Basque Country (UPV/EHU). Valentina Musumeci is grateful to the Initiative of Excellence (IdEX) of the University of Bordeaux for financial support. Mathieu Duttine is thanked for the fruitful discussion on the NMR results. The authors also acknowledge CNRS, Bordeaux INP and Région Nouvelle-Aquitaine for their financial support. This work is partially supported by the Gobierno Vasco-UPV/EHU project IT1246-19 and the Spanish

Ministry of Science, Innovation and Universities projects PCI2019-103657 and RTI2018-098554-B-I00.

Keywords: Supercritical fluids, calcium silicate hydrate nanominerals, nanoconfined water, dielectric spectroscopy, chemical environment

[1] R. Bergman, J. Swenson, *Nature* **2000**, *403*, 283-286.
[2] C. Bakli, S. Chakraborty, *Nanoscale* **2019**, *11*, 11254-11261.
[3] D. Muñoz-Santiburcio, D. Marx, *Chem. Sci.* **2017**, *8*, 3444-3452.
[4] K. Koga, H. Tanaka, X. C. Zeng, *Nature* **2000**, *408*, 564-567.
[5] H. J. Wang, X. K. Xi, X. A. Kleinhammes, Y. Wu, *Science* **2008**, *322*, 80-83.
[6] N. W. Ockwig, J. A. Greathouse, J. S. Durkin, R. T. Cygan, L. L. Daemen, T. M. Nenoff, *J. Am. Chem. Soc.* **2009**, *131*, 8155-8162.
[7] T. H. H. Le, A. Morita, T. Tanaka, *Nanoscale Horiz.* **2020**, *5*, 1016-1024.
[8] G. Algara-Siller, O. Lehtinen, F. C. Wang, R. R. Nair, U. Kaiser, H. A. Wu, A. K. Geim, I. V. Grigorieva, *Nature* **2015**, *519*, 443-445.
[9] M. D. Fayer, M. *Acc. Chem. Res.* **2012**, *45*, 3-14.
[10] S. Xiao, F. Figge, G. Stirnemann, D. Laage, J. A. McGuire, J. *Am. Chem. Soc.* **2016**, *138*, 5551-5560.
[11] G. Goracci, M. Monasterio, H. Jansson, S. Cerveny, *Sci. Rep.* **2017**, *7*, 1-10.
[12] J. S. Dolado, M. Griebel, J. Hamaekers, F. Heber, *J. Mater. Chem.* **2011**, *21*, 4445-4449.
[13] I. G. Richardson, G. W. Groves, *Cem. Concr. Res.* **1992**, *22*, 1001-1010.
[14] S. Cerveny, F. Mallamace, J. Swenson, M. Vogel, L. Xu, *Chem. Rev.* **2016**, *116*, 7608-7625.
[15] J. Swenson, S. Cerveny, *J. Phys. Condens. Matter* **2015**, *27*, 033102.
[16] J. Swenson, H. Jansson, R. Bergman, *Phys. Rev. Lett.* **2006**, *96*, 247802.
[17] V. Samouillan, D. Tintar, C. Lacabanne, *Chem. Phys.* **2011**, *385*, 19-26.
[18] A. Panagopoulou, A. Kyritsis, N. Shinyashiki, P. Pissis, *J. Phys. Chem. B* **2012**, *116*, 4593-4602.
[19] M. Bittelli, M. Flury, K. Roth, K. *Water Resour. Res.* **2004**, *40*, 1-11.
[20] B. Rotenberg, A. Cadéne, J. F. Dufrêche, S. Durand-Vidal, J. C. Badot, P. Turq, *J. Phys. Chem. B* **2005**, *109*, 15548-15557.
[21] R. Bergman, J. Swenson, L. Börjesson, P. Jacobsson, J. *Chem. Phys.* **2000**, *113*, 357-363.
[22] A. Kyritsis, M. Siakantari, A. Vassilikou-Dova, P. Pissis, P. Varotsos, *IEEE Trans. Dielectr. Electr. Insul.* **2000**, *7*, 493-497.
[23] H. Jansson, J. Swenson, *Eur. Phys. J. E* **2003,** *12*, 51-54.
[24] K. Elamin, H. Jansson, J. Swenson, *Phys. Chem. Chem. Phys.* **2015**, *17*, 12978-12987.
[25] L. Frunza, H. Kosslick, I. Pitsch, S. Frunza, A. Schönhals, *J. Phys. Chem. B* **2005**, *109*, 9154-9159.
[26] L. Frunza, A. Schönhals, H. Kosslick, S. Frunza, *Eur. Phys. J. E* **2008**, *26*, 379-386.
[27] M. A. Vasilyeva, Y. A. Gusev, V.G. Shtyrlin, A. Greenbaum, A. Puzenko, P. B. Ishai, Y. Feldman, *Clays Clay Miner.* **2014**, *62*, 62-73.
[28] L. Frunza, H. Kosslick, S. Frunza, R. Fricke, A. Schönhals, J. *Non-Cryst. Solids* **2002**, *307-310*, 503-509.
[29] F. Kremer, A. Schönhals, *Broadband Dielectric Spectroscopy*; Springer-Verlag Berlin Heidelberg, NY, **2003**.
[30] S. Cerveny, S. Arrese-Igor, J. S. Dolado, J. J. Gaitero, A. Alegría, J. Colmenero, *J. Chem. Phys.* **2011**, *134*, 034509.
[31] H. D. Megaw, C. H. Kelsey, *Nature* **1956**, *177*, 390-391.
[32] S. Merlino, E. Bonaccorsi, T. Armbruster, *Eur. J. Mineral.* **2001**, *13*, 577-590.
[33] M. Monasterio, J. J. Gaitero, H. Manzano, J. S. Dolado, S. Cerveny, *Langmuir* **2015**, *31*, 4964-4972.
[34] Y. Kudoh, Y. Takéuchi, *Mineral. J.* **1979**, *9*, 349-373.
[35] L. Black, K. Garbev, *Adv. Appl. Ceram.* **2009**, *108*, 137-144.
[36] C. Hejny, T. Armbruster, *Z. Für Krist. - Cryst. Mater.* **2001**, *216*, 396-408.
[37] G. L. Kalousek, T. Mitsuda, H. F. W. Taylor, *Cem. Concr. Res.* **1977**, *7*, 305-312.
[38] A. R. Grimmer, W. Wieker, *Z. Anorg. Allg. Chem.* **1971**, 34-42.
[39] C. Aymonier, G. Philippot, A. Erriguible, S. Marre, *J. Supercrit. Fluids* **2018**, *134*, 184-196.
[40] A. Loppinet-Serani, C. Aymonier, F. Cansell, J. *Chem. Technol. Biotechnol.* **2010**, *85*, 583-589.
[41] A. Loppinet‐Serani, C. Aymonier, F. Cansell, *Chem. Sus. Chem.* **2008**, *1*, 486-503.
[42] F. Cansell, C. Aymonier, A. Loppinet-Serani, *Curr. Opin. Solid State Mater. Sci.* **2003**, *7*, 331-340.
[43] M. Claverie, M. Diez-Garcia, F. Martin, C. Aymonier, *Chem. Eur. J.* **2019**, *25*, 5814-5823.
[44] F. Cansell, C. Aymonier, *J. Supercrit. Fluids* **2009**, *47*, 508-516.
[45] M. Diez-Garcia, J. J. Gaitero, J. I.; Santos, J. S.; Dolado, J. C. Aymonier, *J. Flow Chem.* **2018**, *8*, 89-95.
[46] M. Diez-Garcia, J. J. Gaitero, J. S. Dolado, C. Aymonier, *Angew. Chem. Int. Ed.* **2017**, *56*, 3162-3167; *Angew. Chem*. **2017**,*129*, 3210-3215.
[47] S. A. S El-Hemaly, T. Mitsuda, H. F. W. Taylor, *Cem. Concr. Res.* **1977**, *7*, 429-438.
[48] T. Mitsuda, K. Sasaki, H. Ishida, *J. Am. Ceram. Soc.* **1992**, *75*, 1858-1863.
[49] X. Huang, D. Jiang, S. Tan, *J. Eur. Ceram. Soc.* **2003**, *23*, 123-126.
[50] K. Lin, J. Chang, G. Chen, M. Ruan, C. Ning, *J. Cryst. Growth* **2007**, *300*, 267-271.
[51] S. V. Churakov, P. Mandaliev, *Cem. Concr. Res.* **2008**, *38*, 300-311.
[52] N. Y. Mostafa, A. A. Shaltout, H. Omar, S. A. Abo-El-Enein, *J. Alloys Compd.* **2009**, *467*, 332-337.
[53] S. Tränkle, D. Jahn, T. Neumann, L. Nicoleau, N. Hüsingb, D. Volkmer, *J. Mater. Chem. A* **2013**, *1*, 10318-10326.
[54] M. Mehrali, E. Moghaddam, S. F. S. Shirazi, S. Baradaran, M. Mehrali, S. T. Latibari, H. S. C. Metselaar, A. Kadri, K. Zandi, N. A. A. Osman, *Appl. Mater. Interfaces* **2014**, *6*, 3947–62.
[55] K. Garbev, P. Stemmermann, L. Black, C. Breen, J. Yarwood, B. Gasharova, *J. Am. Ceram. Soc.* **2007**, *90*, 900-907.
[56] R. L. Frost, M. Mahendran, K. Poologanathan, Y. Xi, *Mater. Res. Bull.* **2012**, *47*, 3644-3649.
[57] K. Garbev, *Struktur, Eigenschaften und Quantitative Rietveldanalyse von Hydrothermal Kristallisierten Calciumsilikathydraten (C–S–H Phasen) - Structure, Properties and Quantitative Rietveld Analysis of Hydrothermal, Crystalline Calcium Silicate Hydrates (C–S–H Phases).* Ph.D. Thesis, University of Heidelberg, Germany, **2004**.
[58] F. Méducin, B. Bresson, N. Lequeux, M. Noirfontaine, H. Zanni, *Cem. Concr. Res.* **2007**, *37*, 631-638.
[59] F. Brunet, Ph. Bertani, Th. Charpentier, A. Nonat, J. Vitlet, *J. Phys. Chem.* B **2004**, *108*, 15494-15502.
[60] H. Rosenberger, A. R. Grimmer, U. Haubenreißer, B. Schnabel, *Magnetic Resonance and Related Phenomena*, Springer, Heidelberg, Berlin, **1979**, p. 106.
[61] I. S. Protsak, Y. M. Morozov, W. Dong, Z. Le, D. Zhang, I. M. A. Henderson, *Nanoscale Res. Lett.* **2019**, 14, 160.
[62] D. Heidemann, W. Wieker, *Nuclear Magnetic Resonance Spectroscopy of Cement-Based Materials*, Springer, Berlin, **2012**, p. 169.
[63] J. P. Yesinowski, H. Eckert, G. R. Rossman, *J. Am. Chem. Soc.* **1988**, *110*, 1367-1375.
[64] C. C. Liu, G. E. Maciel, *J. Am. Chem. Soc.* **1996**, *118*, 5103-5119.
[65] K. S. Cole, R. H. Cole, *J. Chem. Phys.* **1942**, *10*, 98-105.

[66] M. Monasterio, *On the Dielectric Properties of Water Confined in Cement-Like Materials*. Ph.D. Thesis, University of the Basque Country, Spain, **2015**.
[67] S. Cerveny, G. A. Schwartz, J. Otegui, J. Colmenero, J. Loichen, S. Westermann, *J. Phys. Chem. C* **2012**, *116*, 24340-24349.
[68] I. G. Richardson, *Cem. Concr. Res.* **2004**, *34*, 1733-1777.
[69] M. D. Andersen, H. J. Jakobsen, J. Skibsted, *Cem. Concr. Res.* **2004**, *34*, 857-868.
[70] H. F. W. Taylor*, Z. Für Krist. - Cryst. Mater.* **1992**, *202*, 41-50.
[71] H. M. Jennings, *Cem. Concr. Res.* **2000**, *30*, 101-116.
[72] H. Haspel, V. Bugris, Á. Kukovecz, *Langmuir* **2014**, *30*, 1977-1984.
[73] V. Bugris, H. Haspel, A. Kukovecz, Z. Kónya, M. Sipiczki, P. Sipos, I. Pálinko, *Langmuir* **2013**, *29*, 13315-13321.
[74] M. Sulpizi, M.P. Gaigeot, M. Sprik, *J. Chem. Theory Comput.* **2012**, *8*, 1037-1047.
[75] F. J. Jansen, R. A. Schoonheydt, *J. Chem. Soc. Faraday Trans. 1* **1973**, *69*, 1338-1355.

Xonotlite and tobermorite minerals are characterised by layered structures containing hanging Ca-OH and Si-OH groups that interact with confined water molecules. In these systems, the hydrogen bond network and the dynamics of confined water are modified by the presence of different chemical environments. Herein we have shown that the ordered “ice-like” distribution of water molecules found in the Si-OH-rich environments, as in tobermorite, is converted to a disordered “liquid-like” distribution in the Ca-OH-rich environment in xonotlite.